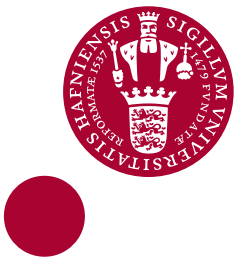

Chromosome copy number variation in telomerized human bone marrow stromal cells; insights for monitoring safe ex-vivo expansion of adult stem cells

Burns, Jorge S.; Harkness, Linda; Aldahmash, Abdullah; Gautier, Laurent; Kassem, Moustapha

Published in:
Stem Cell Research

DOI:
10.1016/j.scr.2017.09.006

Publication date:
2017

Document version
Publisher's PDF, also known as Version of record

Stem Cell Research 25 (2017) 6–17

Contents lists available at ScienceDirect

Stem Cell Research

journal homepage: www.elsevier.com/locate/scr

Chromosome copy number variation in telomerized human bone marrow stromal cells; insights for monitoring safe *ex-vivo* expansion of adult stem cells

Jorge S. Burns [a,b,*], Linda Harkness [a,c], Abdullah Aldahmash [a,d], Laurent Gautier [e], Moustapha Kassem [a,f,g,h]

[a] Department of Endocrinology and Metabolism, University Hospital of Odense, DK-5000 Odense C, Denmark.
[b] Laboratory of Cell Biology and Advanced Cancer Therapies, Department of Oncology Hematology and Respiratory Disease, University Hospital of Modena and Reggio Emilia, Modena, Italy
[c] Australian Institute for Bioengineering and Nanotechnology, University of Queensland, Brisbane, QLD, Australia
[d] College of Medicine, Department of Anatomy, Stem Cell Unit, King Saud University, Riyadh 11461, Saudi Arabia
[e] Center for Biological Sequence Analysis/DTU Multi Assay Core, Department for Systems Biology, Technical University of Denmark, DK-2800 Lyngby, Denmark
[f] Institute of Cellular and Molecular Medicine & DanStem, Panum Institute, University of Copenhagen, Copenhagen, Denmark
[g] Department of Cellular and Molecular Medicine, The NovoNordisk Center for Stem Cell Biology (DanStem), University of Copenhagen, Copenhagen, Denmark
[h] Stem Cell Unit, Department of Anatomy, College of Medicine, King Saud University, Saudi Arabia

ARTICLE INFO

Article history:
Received 24 April 2017
Received in revised form 14 July 2017
Accepted 20 September 2017
Available online 25 September 2017

Keywords:
Karyotype
Bone marrow stromal cell
Sky
Array CGH

ABSTRACT

Adult human bone marrow stromal cells (hBMSC) cultured for cell therapy require evaluation of potency and stability for safe use. Chromosomal aberrations upsetting genomic integrity in such cells have been contrastingly described as "Limited" or "Significant". Previously reported stepwise acquisition of a spontaneous neoplastic phenotype during three-year continuous culture of telomerized cells (hBMSC-TERT20) didn't alter a diploid karyotype measured by spectral karyotype analysis (SKY). Such screening may not adequately monitor abnormal and potentially tumorigenic hBMSC in clinical scenarios. We here used array comparative genomic hybridization (aCGH) to more stringently compare non-tumorigenic parental hBMSC-TERT strains with their tumorigenic subcloned populations. Confirmation of a known chromosome 9p21 microdeletion at locus *CDKN2A/B*, showed it also impinged upon the adjacent *MTAP* gene. Compared to reference diploid human fibroblast genomic DNA, the non-tumorigenic hBMSC-TERT4 cells had a copy number variation (CNV) in at least 14 independent loci. The pre-tumorigenic hBMSC-TERT20 cell strain had further CNV including 1q44 gain enhancing *SMYD3* expression and 11q13.1 loss downregulating *MUS81* expression. Bioinformatic analysis of gene products reflecting 11p15.5 CNV gain in tumorigenic hBMSC-TERT20 cells highlighted networks implicated in tumorigenic progression involving cell cycle control and mis-match repair. We provide novel biomarkers for prospective risk assessment of expanded stem cell cultures.

1. Introduction

Successful trials showing autologous stem cell subpopulations isolated from human adult bone marrow tissue can be grown *ex vivo* and subsequently reintroduced into patients to improve regenerative repair of large bone defects (Quarto et al., 2001) have prompted need for standardized protocols to broaden the therapeutic scope (Panchalingam et al., 2015). Associated with optimal cell sourcing approaches and cell dosage requirements, the monitoring of procedural risk is of fundamental concern. Cultured cells are susceptible to stochastic acquisition of hereditable changes that may subvert function or introduce a detrimental outcome. Oncogenic changes can be monitored with very sensitive specific techniques, yet the wide diversity of potential aberrations can confound analysis and suitable biomarkers in the context of expanded "hBMSC" populations have yet to be defined. Significant oncogenic changes can range from discrete single codon mutations, gene amplification, loss of tumor suppressor gene function and epigenetic modifications. Since such changes usually reflect or evoke chromosome abnormalities, it was reasonable to propose that karyotypic analysis might suffice to provide an overview of whether the expanded stem cells are fit for therapeutic use (Saito et al., 2011), although this view has raised controversy (Ferreira et al., 2012).

As a model system exemplifying accumulated genetic instability in long-term continuously expanded cell cultures, we previously reported that telomerized human bone marrow stromal cell strains hBMSC-TERT (aka "hMSC-TERT"), ordinarily forming heterotopic bone when transplanted with osteoconductive scaffold into immune deficient mice

* Corresponding author at: Laboratory of Cell Biology and Advanced Cancer Therapies, Department of Oncology Hematology and Respiratory Disease, University Hospital of Modena and Reggio Emilia, Modena, Italy.
E-mail address: Jorge.Burns@Unimore.it (J.S. Burns).

https://doi.org/10.1016/j.scr.2017.09.006

(Simonsen et al., 2002), could eventually spontaneously evolve a neoplastic phenotype (Serakinci et al., 2004). Notably, however, the tumorigenic cells retained a normal diploid karyotype (Burns et al., 2008). To improve detection of cytogenetic changes in cultured cells, we hereby describe use of array comparative genomic hybridization (aCGH) to identify segments of the genome existing as different copy number variants (CNV). A reference human diploid fibroblast genomic DNA was compared to bone-forming hBMSC-TERT4 and hBMSC-TERT20 cell strains, versus six sub-cloned tumorigenic cell lines derived from the extended culture neoplastic hBMSC-TERT20 strain of high population doubling level (PDL) (Burns et al., 2005). Inclusion of single-cell derived clones in our comparative analysis was advantageous, since aCGH may fail to detect low-level mosaicism (≤10%) among a heterogeneous cell strain (Elliott et al., 2010). Use of a progressive cell model with comprehensively measured growth kinetics in closely matched cell strains allowed verification of CNV reproducibility. The capacity to correlate genetic aberrations with population doubling level and acquisition of a tumorigenic phenotype, helped identify specific CNV more likely to harbour potentially causative genetic changes. Furthermore, prior cytohistological data for cancer and differentiation pathway proteins in hBMSC-TERT20 populations provided a verified context for exploring the potential relevance of CNV-associated genes. A biological database search tool for interacting genes/proteins confirmed that many CNV-specific genes were highly germane for tumorigenic progression, sharing relevance with events prevalent in human cancers and sarcomas.

2. Materials and methods

2.1. Cell culture

From concern that broad casual use of the term MSC can introduce confusion (Robey, 2017; Caplan, 2017) cells called “hMSC-TERT” in our prior publications are here renamed hBMSC-TERT. The hBMSC strain were cultured from a healthy male donor, 46, XY (age 33) transduced at population doubling level (PDL) 12 with a retroviral vector overexpressing the human telomerase reverse transcriptase gene (hBMSC-TERT cells) was used to derive the hBMSC-TERT2, hBMSC-TERT4 and hBMSC-TERT20 populations. Notably, the hTERT vector wasn't tagged with an independent co-selectable marker, thus selection relied purely on hTERT function driving growth beyond the senescence observed in untransduced control primary hBMSC. As previously described (Abdallah et al., 2005), eight passages after retroviral transduction (PDL 23), cells were partitioned into two passage regimes, with split ratios of 1:2 or 1:4 to generate hBMSC-TERT2 or hBMSC-TERT4 populations. By PDL 47, hBMSC-TERT4 cells were further partitioned into a 1:20 split ratio hBMSC-TERT20 population. Cell number was calculated for each weekly passage. Prior analysis of neoplasia detected loss of the $p16^{INK4A}$/ARF locus in both hBMSC-TERT4 and hBMSC-TERT20 cells, plus *Kras* Q61H mutation specific to hBMSC-TERT4 cells and oncogene methylation of the *DBCCR1*/*DBC1*/*BRINP1* promoter specific to hBMSC-TERT20 cells (Serakinci et al., 2004). At late passage (PDL 440), hBMSC-TERT20 was used to derive single-cell sub-clones designated -BB3, -BC8, -BD6, -BD11, CE8 and DB9 as described (Burns et al., 2005). Subsequent histological analysis of hBMSC-TERT20 strains and subclones examined a panel of cancer pathway prognostic biomarkers (Burns et al., 2008). All cells were grown in phenol red-free minimal essential medium (MEM) supplemented with 10% batch-tested fetal bovine serum (FBS) and 1% penicillin/streptomycin (Gibco Invitrogen) and maintained in a 5% CO2 humidified incubator at 37 °C.

2.2. Array-based Comparative Genomic Hybridization (aCGH)

Genomic DNA was prepared using the Puregene DNA Purification Kit (Qiagen). aCGH was performed following the standard Agilent protocol (V6.1). Briefly, 700 ng of hBMSC-TERT lineage cell genomic DNA and 700 ng of reference diploid human fibroblast genomic DNA 46,XX was digested with *Alu*I and *Rsa*I and labeled with Cy5- or Cy3-dUTP (Agilent). Following purification with Microcon YM-30 filters (Millipore), the labeled DNA yield and quality was checked on a NanoDrop ND- 1000 UV-VIS Spectrophotometer (Thermo Fisher Scientific, Waltham, MA, USA) and Agilent 2100 Bioanalyzer using Bioanalyzer DNA High Sensitivity (Agilent Technologies). The labeled samples were hybridized at 65 °C on Agilent dual colour arrays (Sureprint G3, 2x400k cat.#G4825A; Agilent Technologies) for 24 h in a rotator oven at 20 rpm. The annotation files corresponded to NCBI build 36.1 of the human genome hg18 (March 2006) containing 411,056 60-mer probes. The comprehensive probe coverage allowed genome-wide DNA CNV profiling focused on known genes, promoters, miRNAs, pseudoautosomal and telomeric regions. Slides were washed according to the protocol and scanned immediately at 2 μM resolution on an Agilent G2565CA high-resolution scanner. Data was extracted using Agilent Feature Extraction software and the resulting files were processed with the Bioconductor limma package version 2.18.2, with the raw data cleaned for background noise using the normexp convolution model. The resulting signal was processed using a quantiles-based normalization procedure. Figures were generated with help of R software ggplot2 implementation of the Grammar of Graphics.

2.3. RT-PCR Analysis of gene expression

Cellular RNA from hBMSC-TERT4 PDL-175 and hBMSC-TERT20 PDL-337 was isolated using a single-step method with TRIzol (Invitrogen, Taastrup, Denmark) according to manufacturer's instructions. First-strand complementary cDNA was synthesized from 4 μg of total RNA in accordance to a Revertaid H minus first-strand cDNA synthesis kit (Fermentas). Real-time polymerase chain reaction (RT-PCR) utilized the StepOne PlusTM RT-PCR system (Applied Biosystems) with double-strand DNA-specific SYBR → Green I luminescent dye. In a total reaction volume of 10 μL, 20 pmol/mL of each primer (DNA Technology A/S or Eurofins, Ebersberg, Germany) and 10 pmol/mL for each reference gene was used with Fast SYBR® Green master mix (ABI). The cycle conditions included an initial denaturation step at 95 °C for 20 s and 40 cycles of 95 °C for 3 s, and 60 °C for 30 s. Normalization was achieved via the reference gene β2-microglobulin (Lupberger et al., 2002) (primer sequences in Supplementary Table 1).

In vivo xenograft of hBMSC-TERT cells in immuno-deficient mice hBMSC-TERT4 PDL 192 cells (5×10^5) combined with hydroxyl- apatite/tricalcium phosphate 1–2 mm diameter granules (HA/β-TCP, 40 mg, Zimmer Scandinavia, Denmark) were transplanted subcutaneously into the dorsum of 8-week- old female NOD/SCID mice (NOD/LtSz-Prkdcscid) as described (Burns et al., 2010). The transplants were recovered eight weeks after transplantation, transferred to 4% neutral buffered formalin for about 45 min, and then formic acid was added for 2 days. Adopting standard histopathologic methods, the HA/β-TCP implants were embedded in paraffin and 4-μm tissue sections were stained with hematoxylin and eosin Y (H&E) (Bie & Berntsens Reagenslaboratorium). Similarly, tumorigenic hBMSC-TERT20 PDL 480 cells (5×10^5) combined with Matrigel™ were transplanted subcutaneously into the murine dorsal region and recovered two weeks after transplantation, fixed in 4% neutral buffered formalin as above and embedded in paraffin for subsequent H&E staining of 4-μm tissue sections.

2.4. Bioinformatic characterization of copy number variable genes

To explore CNV relevance to known hBMSC-TERT cell biology, we referenced prior molecular studies of tumorigenic events, including genetic abnormalities and the expression of proteins involved in pathways to cancer, the cell cycle, DNA mismatch repair and ossification. Associations between such hBMSC-TERT qualified molecules and CNVs were made using the Search Tool for Retrieval of Interacting Genes/Proteins database (STRING, version 10.0), a database comprised known and predicted interactions, including direct (physical) and indirect (functional)

associations based on genomic context, high throughput experiments, conserved co-expression and previous knowledge (Szklarczyk et al., 2015). In the first instance, we mapped CNV associated with experimentally known hBMSC-TERT pathways in cancer. Subsequently, to confirm the significance of CNV specific to preneoplastic hBMSC-TERT20 cells, software-derived high confidence 1st shell network interactors to SMYD3 (SET and MYND domain- containing protein 3) and SIRT1 (Sirtuin 1) were used to map further CNV target associations in epigenetic pathways. Software clustering tools included KEGG pathway enrichment (Kanehisa et al., 2016).

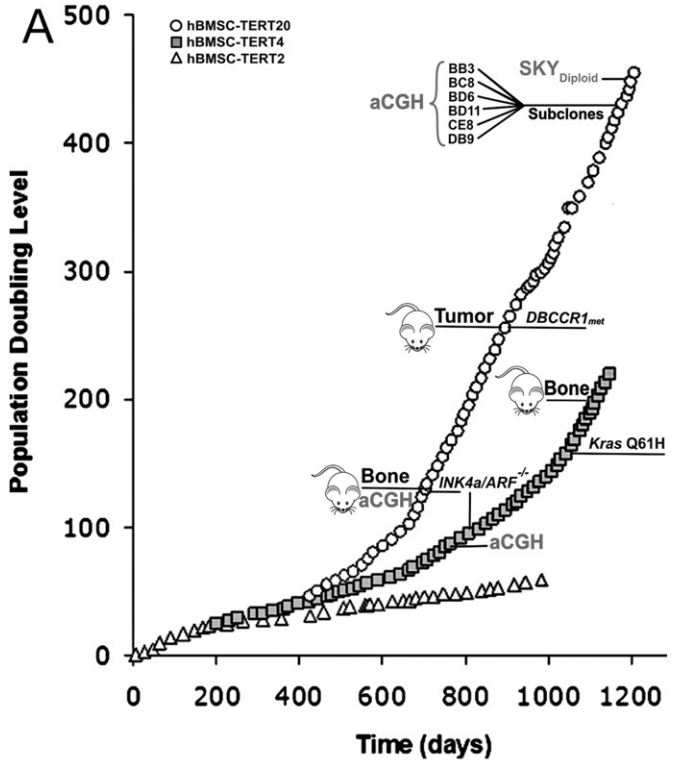

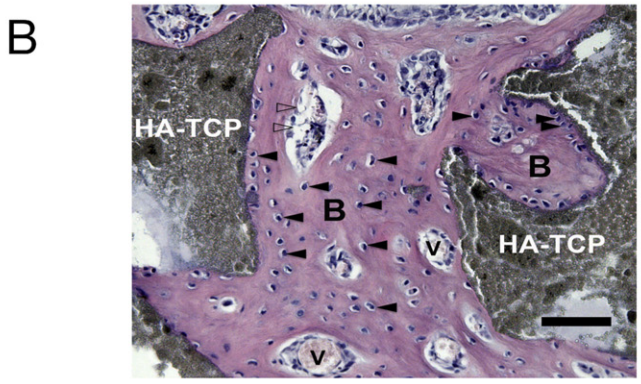

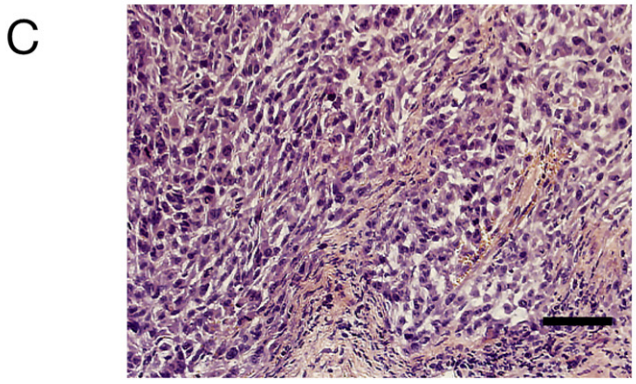

2.5. Statistical analysis

For the real-time PCR analysis, a two-tailed *t*-test was applied to analyze the expression of the CNV target genes in different hBMSC-TERT cell populations. Fold-changes in gene expression between samples with p values < 0.05 were considered significant. The STRING v10 database clustering coefficient for interactions assumed a statistical background of the whole genome.

3. Results

3.1. Cell growth kinetics; passage split ratio associated tumorigenicity

As reported, the subculture passage split ratio was an extrinsic factor that influenced hBMSC-TERT cell growth rates and led to three passage split ratio-specific growth curves (Fig. 1A). hBMSC-TERT20 cells, passaged 1:20, showed the greatest step-wise acceleration in growth rate, leading to a consistent DT of only 1.4 days by PDL-256, the point in their evolution when xenografts were tumorigenic. Propagated with a 1:4 passage split ratio, hBMSC-TERT4 cells evolved doubling time changes during passage from 4.6 days at PDL-74, to 4.2 days at PDL-95 and 1.5 days at PDL-169. The higher 1:4 seeding density for hBMSC-TERT4 influenced culture contact inhibition (Abercrombie, 1970) since cells were promptly in contact with each other after just one division. In contrast, even 24 h after seeding, 1:20 split hBMSC-TERT20 cells were distributed more autonomously on the culture surface. Previously detected genetic and epigenetic aberrations discovered in the hBMSC-TERT strains included a *Kras* Q61H oncogene activation detected in hBMSC-TERT4 cells at PDL-169. At the time, we reported that hBMSC-TERT4 cells at PDL-169 were nevertheless not tumorigenic. Confirming this was indeed the case, PDL 192 hBMSC-TERT4 cells subcutaneously transplanted with osteoconductive scaffold, formed a trabecular bone matrix tissue after 8 weeks in immune compromised mice, $n = 4/4$ (Fig. 1B). Thus, we were confident of comparing non-tumorigenic (hBMSC-TERT4 and early hBMSC-TERT20 populations) versus tumorigenic phenotypes (high PDL hBMSC-TERT20 subclones) when interpreting the CNV observations.

3.2. Genetic aberrations confirmed and discovered by array CGH

To generate array CGH profiles, glass slide anchored probes of known mapped sequences representing homogenous regions in the genome, competitively bound two samples of "reference" versus "test" genomic DNA, each labeled with differentiating fluorescent dyes. Consequently, copy number could be indirectly calculated from a ratio

Fig. 1. A, Long term growth curves of three independently grown, split ratio-specific, cell populations derived from hBMSC-TERT cells in continuous culture for over 3 years. (△) hBMSC-TERT2, passage split ratio 1:2; (■) hBMSC-TERT4, passage split ratio 1:4; (○) hBMSC-TERT20, passage split ratio 1:20. Cell number was calculated weekly over the indicated period. Time points indicate known genetic aberrations (Ink4a/ARF deletion, Kras Q61H mutation and DBCCR1 methylation silencing), xenograft outcomes (bone or tumor), array comparative genomic hybridization (aCGH) sampling, single cell subclones derivation by limiting dilution and hBMSC-TERT20 spectral karyotyping (SKY). B, Heterotopic bone formation by K-ras Q61H mutant hBMSC-TERT4 cells. Histological analysis of 4 μm sections of decalcified paraffin embedded implants harvested 8 weeks after subcutaneous transplantation of hBMSC-TERT4 PDL-192 cells with hydroxyapatite-tricalcium phosphate (HA-TCP) granules in immunodeficient mice. Hematoxylin and eosin pink stained new trabecular bone matrix, (B) within the HA-TCP scaffold, contained numerous osteocytes within lacunae (solid arrows) and blood vessels (v) with adipocytes (open arrows) adjacent to haematopoietic cells (h). C, Sarcoma formation by hBMSC-TERT20 cells. Histological analysis of 4 μm sections of xenografts harvested two weeks after subcutaneous transplantation of hBMSC-TERT20 PDL-480 cells with Matrigel™. Scale bar = 100 μm.

of fluorochrome intensities proportional to the relative probe-spanning chromosome abundance of the samples. Profiles for each chromosome comprised a ranking of $\log_2$ fluorescent ratios plotted according to the probe's corresponding physical position on the genome. The plotted data were normalized with a median set to log2(ratio) = 0 for regions of no change; positive means represented duplicated whilst negative means represented deleted regions in the test genome. Since results were based on fluorescent measurement, the signal was plotted as continuous even if the underlying biological process was discrete (relative copy numbers of DNA sequences). N.B. The relative copy number value in the test sample could vary due to heterogeneous incidence in the cell population. For confidence, aberrations with a minimum of four probes in the region were chosen. One exception, at 11q13.1 had an individual probe with a particularly strong signal reproduced in most test samples. With very characteristic profile patterns, the hBMSC-TERT strains and isogenic expanded subclones confirmed the very high reproducibility of the aCGH approach. Microdeletions in chromosome regions 1q21.1, 2q11.2, 2q21.1, 3q26.1, 9p21.3, 11p15.1, 15q24.2, 17q23.2, 21q11.2 and 22q11.23 were ubiquitous in both hBMSC-TERT substrains and all subclones. The known $p16^{INKa}$/ARF microdeletion at 9p21.3, one of the clearest aberrations found (Fig. 2A), was now better defined by 30 consecutive probes spanning the CDKN2A, CDKN2B and adjacent MTAP loci (Fig. 2B). The CNV profile indicated the span of chromosome loss was the same for hBMSC-TERT4, hBMSC-TERT20 and all the hBMSC-TERT20 subclones. The 9p21.3 CNV seen in hBMSC-TERT4 had a probe deletion ratio range (−1 to −3) that was substituted by a narrower range of larger ratios (−2 to −3) in hBMSC-TERT20 cells and subclones, likely indicative of accrued missing genomic segments. For the non-ubiquitous CNV, restricted to more specific cell populations, there was a tendency for the CNV ratio between sample and control to be 1.

To more closely correlate CNV to the tumorigenic phenotype, we focused on CNV specific to the hBMSC-TERT20 strain and its tumorigenic subclones (Table 1). Notably, two CNV absent in non-tumorigenic hBMSC-TERT4 PDL 88 cells were found in the pre-tumorigenic hBMSC-TERT20 PDL116 population and subsequent hBMSC-TERT20 PDL440 derived tumorigenic subclones; namely, a 1q44 gain (Fig. 3A) and a microdeletion at 11q13.1 (Fig. 3B). The region concerning CNV 1q44 co-involved two probes targeting *SMYD3* that encodes a histone methyltransferase involved in the proliferation of cancer cells (Hamamoto et al., 2004). The region lost by CNV 11q13.1 co-involved *MUS81*, a crossover junction endonuclease. RT-PCR analysis of gene expression in hBMSC-TERT4 PDL 175 versus hBMSC-TERT20 PDL 337 confirmed that changes in relative expression agreed with expectations from the corresponding CNV type. This was not the case for a more centromeric chromosome 11 control gene *MAP3K11* outside the CNV region (Fig. 3C). The chromosome showing most imbalances and CNV was chromosome 11. Specific to all tumorigenic hBMSC-TERT20 subclones we observed amplification of the short (p) arm of chromosome 11 at the telomeric region 11p15.5 (chr11:0–570,000) (Fig. 4A) comprising 37 genes from *IFITM5* to *PHRF1* including *HRAS* (Fig. 4B). This region didn't involve a centromerically distal neighboring cluster of imprinted

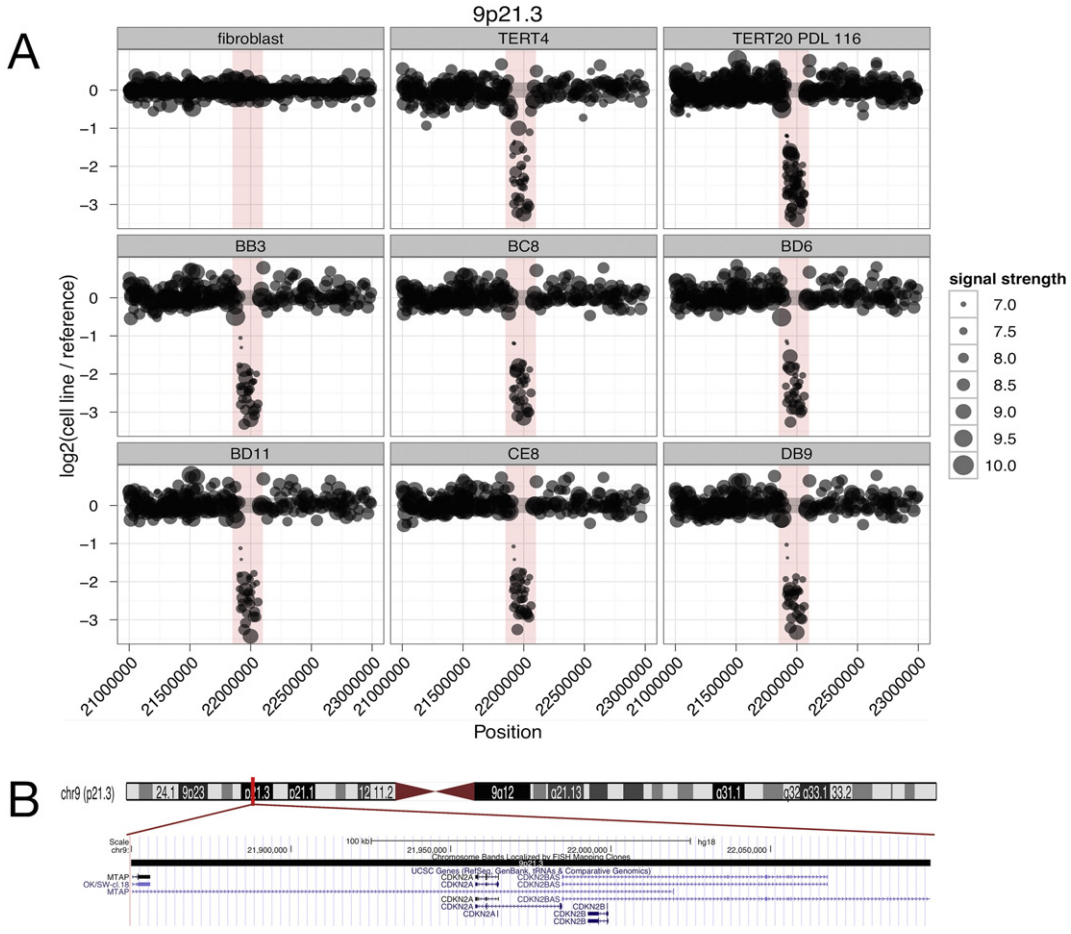

Fig. 2. Array CGH profile of chromosome subregion in hBMSC-TERT strains and subclones. A, The 9p21.3 deletion included multiple probes spanning a locus for *CDKN2A*, *CDKN2B* and exon 8 of *MTAP*. Abscissa: Location of the probe on the genome. Ordinate: The log-ratio of the aCGH probe signal for sample versus reference genomic DNA. Positive and negative log-ratios indicated amplification or deletion respectively, ±1 indicates a gain or loss of one of the two alleles, larger -log ratios indicate missing genomic segments. Plotted dot size is proportional to overall intensity of the probe signal. B, Chromosome 9 ideogram, red bar highlights the 9p21.3–250 kbp CNV region with UCSC database annotation for genes spanned by chr9:21,850,000–22,100,000. Opposing red arrowheads represent the centrosomic region.

Table 1
CNV in bone-forming hBMSC-TERT4 and hBMSC-TERT20 strains, versus hBMSC-TERT20 tumorigenic subclones.

Cytoband locus	Copy number variation	CNV size	hBMSC-TERT4	hBMSC-TERT20	hBMSC-TERT20					
	(CNV)	(kbp)	PDL 88	PDL 116	BB3	BC8	BD6	BD11	CE8	DB9
1q21.1	Loss	1000	+	+	+	+	+	+	+	+
1q44	Gain	300		+	+	+	+	+	+	+
2q11.2	Loss	100	+	+	+	+	+	+	+	+
2q21.1	Loss	225	+	+	+	+	+	+	+	+
3q26.1	Loss	120	+	+	+	+	+	+	+	+
6q23.3	Loss	110								+
9p21.3	Loss	250	+	+	+	+	+	+	+	+
11p15.5-q25	Gain	135,000							+	
11p15.5	Gain	570			+	+	+	+	+	+
11p15.4	Loss	400						+		
11p15.1	Loss	40	+	+	+	+	+	+	+	+
11q13.1 (a)[a]	Loss	15		+	+	+	+	+	+	+
11q13.1 (b)[a]	Loss	65					+			
15q24.2	Loss	5	+	+	+	+	+	+	+	+
17q23.2	Loss	50	+	+	+	+	+	+	+	+
21q11.2	Loss	600	+							
22q1123	Loss	30	+	+	+	+	+	+	+	+
Xq21.33	Loss	60								+

[a] (a) chr11:65,375,000–65,390,000 (b) chr11:65,550,000–65,620,000.

genes associated with Beckwith-Wiedemann syndrome (BWS) and a high risk of development of childhood sarcomas. Nonetheless, the BWS region may remain relevant for sub-clone–CE8, since the CNV log2 ratio for this particular clone was consistently 0.5 higher than the other sub-clones, indicative of a full chromosome 11 imbalance. Our analysis restricting the 11p15.5 amplified region window to chr11:0–1000,000 to comprise at least a further 32 influenced genes (Fig. 4C), was most likely a conservative estimate for hBMSC-TERT20-CE8.

3.3. Interacting Genes/Proteins suggest a CNV role in tumorigenesis

Tumorigenic events characterized from previous studies exploring events in hBMSC-TERT20 cell tumorigenic progression (Serakinci et al., 2004) (Burns et al., 2005) (Burns et al., 2008), provided a contextual framework for exploring CNV relevance. The principle aspects of the contextual framework could be described as follows: Driving hBMSC-TERT characteristics, hTERT associated with many genes and proteins belonging to KEGG pathways in cancer, including cell cycle regulators; both CDKN2A gene locus products p16INK4a and alternate reading frame $p14^{arf}$, the CDKN2B gene product $p15^{INK4B}$, the CDKN1A gene product $p21^{Cip1}$, the CDKN1B product $p27^{Kip1}$, CCND1 derived Cyclin D1 and tumor suppressor gene products RB1 and TP53 as well as cell surface receptors EGFR and VEGFA. The latter two trophic factor receptors also interacted with TP53 that in turn interacted with a series of mismatch repair proteins MLH1, MSH2, PMS2 and MSH6 to establish a cardinal role for TP53 in regulating cell cycle activity and conserving genomic stability. The cell cycle machinery interacts with cytoskeleton dynamics, reflecting important external cues such as cell-cell or cell-matrix adhesions that modulate activity of the cell autonomous proliferation machinery through specific checkpoints. In turn, changes in extracellular matrix organisation involving CD44, COL4A1, SPARC, COL1A1, IBSP and BGN are key aspects of ossification.

In addition to the CNV already mentioned above; 1q44, 9p21.3, 11p15.5 and 11q13.1, a further six CNV at 1q21.1, 2q11.2, 2q21.1, 11q13.1 (-BD6 specific), 17q23.21 and 22q11.23 (Fig. 5A–F), spanned genes that could interact directly with the hBMSC-TERT contextual framework in a manner shown schematically in Fig. 6A. This string database interaction map for the hBMSC-TERT contextual framework had an overall clustering coefficient of 0.794 and more interactions than would be predicted from chance, indicating the CNV were likely to be biologically connected to tumorigenic events found in hBMSC-TERT20 cells. As many as twenty CNV-specific interactors recruited in this network were from the 23 STRING identified proteins within the 11p15.5 CNV chromosome gain locus, including a cluster of genes encoding interferon-induced transmembrane protein family members. In contrast, for the ubiquitous 1q21.1 CNV loss that also harbored 37 Refseq coding sequences, including non-annotated genes, only six were identified by the STRING database of which just two, PPIAL4C and NBPF10, interacted with the network. A KEGG pathway analysis of the network indicated that ten of the a priori defined contextual network proteins (CCND1, CDKN1A, CDKN1B, COL1A1, COL4A1, EGFR, IBSP, LAMA1, TP53, VEGFA) were components of the PI3K/AKT/mTOR signaling network important for regulating the cell cycle. Notably, four hypothetical gene products from the 11p15.5 CNV specific to the tumorigenic hBMSC-TERT20 sub-clones (AP2A2, PSMD13, SIRT3 and HRAS), interacted with this pathway. Moreover, it was possible to derive additional networks more specifically related to SMYD3 (Fig. 6B) and epigenetic signaling (Fig. 6C) (a total of 38 highly predicted functional network partners from a total of 67 STRING identified gene products).

3.4. Evidence for CNV contributions to epigenetic deregulation

The STRING database for the contextual framework above didn't indicate a direct interaction for the 1q44 CNV gain candidate gene SET and MYND domain-containing protein 3 (SMYD3). Yet its relevance can be predicted, as acetylation of the histone H3 TERT promoter region is one of several targets for this histone methyltransferase (Liu et al., 2007), a principal epigenetic modification of chromatin that can determine gene expression, genomic stability and cell mitosis. Thus, STRING was used to identify 10 highly predicted SMYD3 partners, forming a contextual framework for exploring SMYD3-related CNV relevance. Eight SMYD3 predicted functional network partners directly interacted with 13 predicted proteins from 58 STRING identified target genes spanned by 6 CNV. Notably, the network involved the 9p21.3 CNV genes and most of the highly predicted SMYD3 functional network partners interacted with HRAS from the 11p15.5 CNV (Fig. 6B).

Fig. 3. CNV specific for pre-tumorigenic hBMSC-TERT20 cells and tumorigenic subclones. A, Array CGH profile for 1q44 in each cell type. Axes as described in Fig. 2. Plotted dot size proportional to overall intensity of the probe signal. Chromosome 1 ideogram, red bar highlights the 1q44 ~ 300 kbp CNV region spanning USCC database annotated genes SMYD3, TFB2M and chromosome 1 open reading frame 71, C1orf71/consortin within chr1: 244,500,000–244,800,000. B, Array CGH profile for 11q13.1 in each cell type. Chromosome 11 ideogram, red bar highlights the 11p13.1–15 kbp CNV region spanning USCC database annotated genes SNX32, CFL1 and MUS81 within chr11:65,555,000–65,620,000. C, RT-PCR analysis for expression of 1q44 CNV SMYD3 gene, 11q13.1 MUS81 and a neighboring 11q13.1 gene outside the CNV region, MAP3K11. (*$p < 0.05$). Opposing red arrowheads represent the centrosomic region.

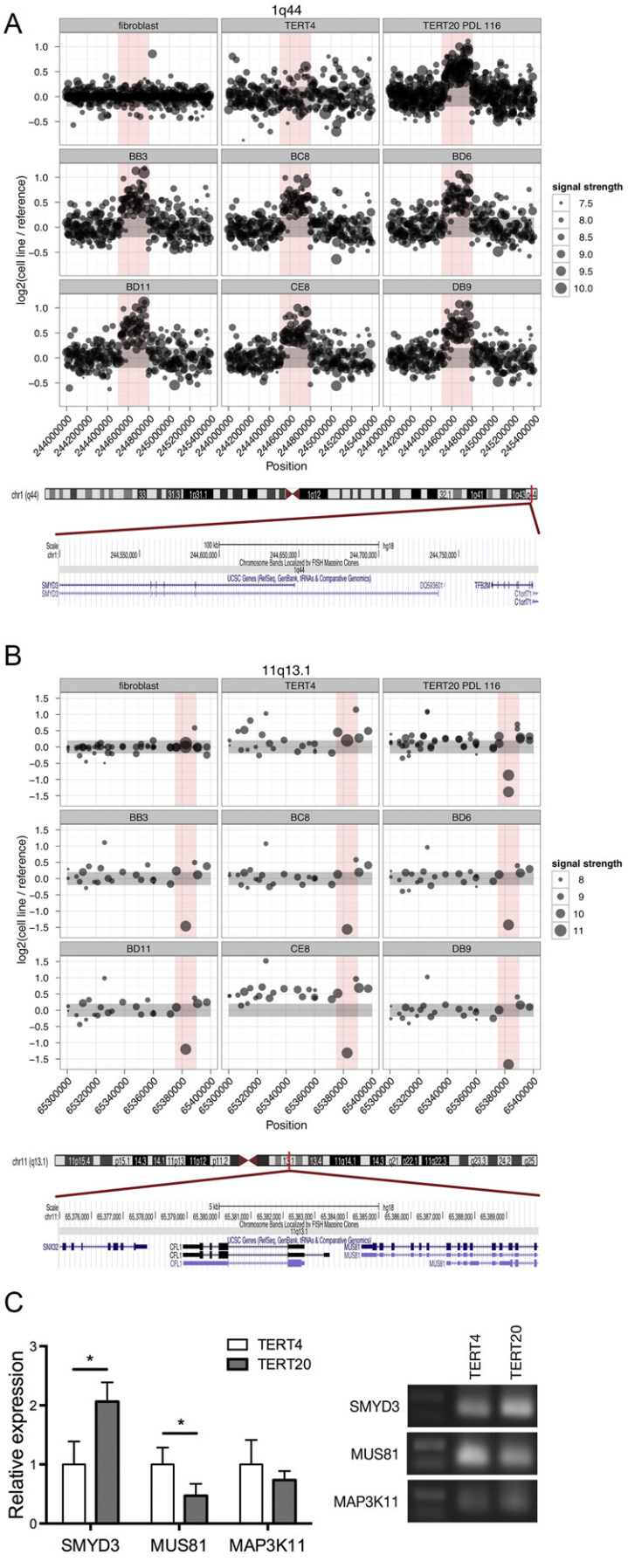
A
1q44
fibroblast
TERT4
TERT20 PDL 116
BB3
BC8
BD6
BD11
CE8
DB9
log2(cell line / reference)
signal strength
7.5
8.0
8.5
9.0
9.5
10.0
Position
B
11q13.1
signal strength
8
9
10
11
C
Relative expression
TERT4
TERT20
SMYD3
MUS81
MAP3K11

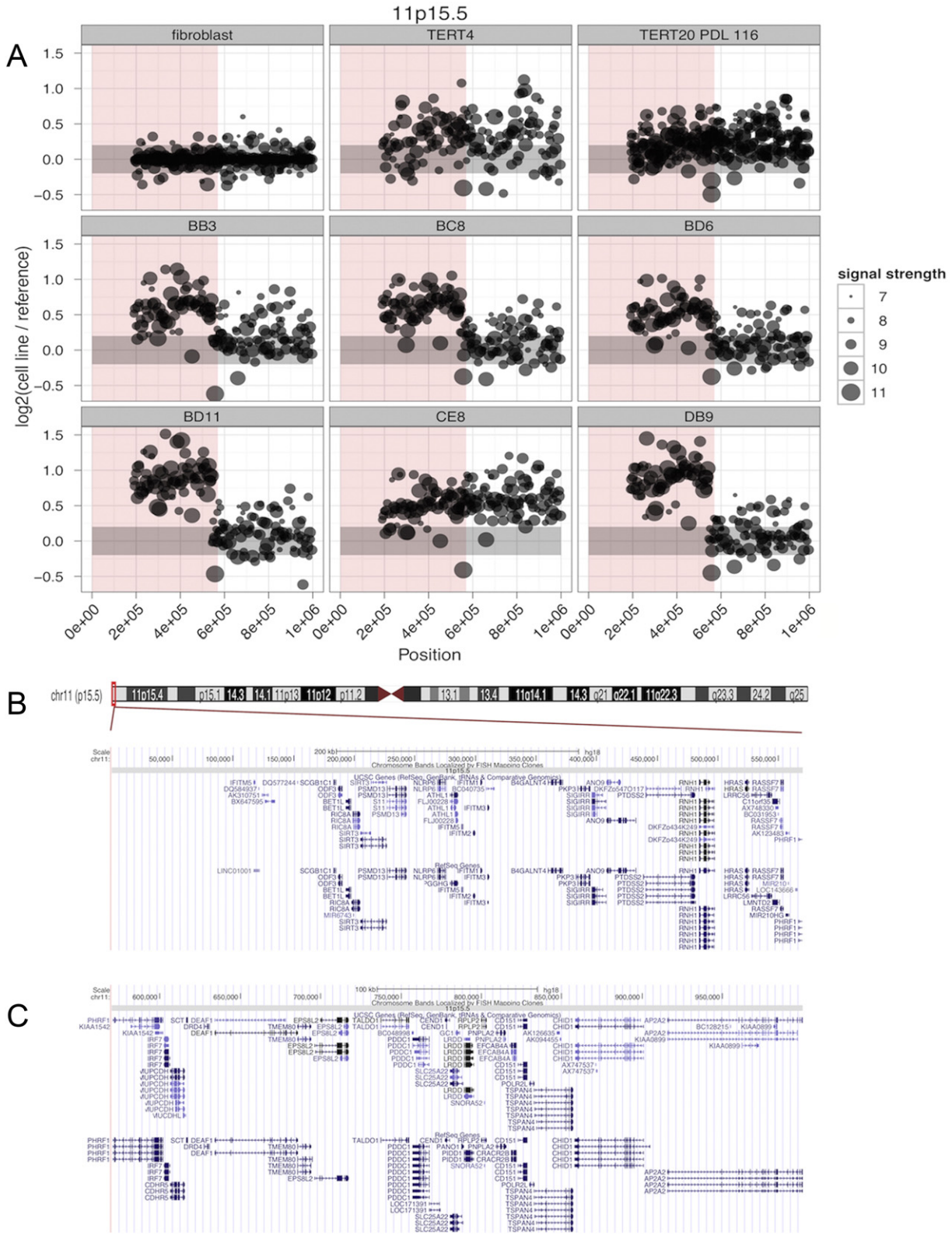

Fig. 4. CNV specific for hBMSC-TERT20 tumorigenic subclones. A, Array CGH profile for 11p15.5 in each cell type. Axes as described in Fig. 2. Plotted dot size proportional to overall intensity of the probe signal. B, Chromosome 11 ideogram, red bar highlights the 11p15.5 ~ 570 kbp CNV spanning USCC and Refseq database annotated genes including HRAS within chr11:0–570,000. C, Chromosome 11 ideogram, red bar highlights the 11p15.5 ~ 450 kbp CNV specific to clone –CE8 cells spanning USCC and Refseq database annotated genes including PIDD, POLR2L and CD151 within chr11:570,000–1000,000. This was a conservative estimate, CE8 CNV indicated whole chromosome 11 imbalance. Opposing red arrowheads represent the centrosomic region.

The histone NAD dependent protein deacetylase Sirtuin (SIRT1) is another epigenetic regulator of telomeric maintenance and highly relevant to cell cycle, DNA repair and apoptosis, linking transcriptional regulation directly to intracellular energetics. Using STRING to identify highly predicted SIRT1 partners resulted in a contextual framework incorporating 19 predicted proteins from 59 STRING identified genes spanned by nine different CNV loci, again including the 9p21.3 CNV targets CDNK2A and CDKN2B that ordinarily inhibit histone acetylation

(Fig. 6C). Thus, a high proportion of the STRING database identified CNV candidate genes interacted with molecules known to have a key role in epigenetic modulation (57% in the hBMSC-TERT contextual network derived from prior experimental data, 22% in a SMYD3 network, and 32% in a SIRT1 network) representing effector proteins with critical roles in cell signaling networks.

4. Discussion

A typical workflow for stem cell-based therapy includes stem cell isolation, expansion, manipulation, preclinical evaluation, engraftment and follow-up. Even promising alternative "non-whole cell" therapeutic strategies e.g. decellularized matrix (Yam et al., 2016), extracellular vesicles (György et al., 2015) or targeted epigenetic conversion of endogenous cells (Black et al., 2016), are unlikely to totally replace whole cells as advanced therapy medical products (ATMP). Genetic drift of cultured cells for any therapeutic product will remain of major concern regarding consistency, functional efficacy and safety (Furlani et al., 2009). Traditional *in vivo* tumorigenicity assays can be incompatible with recommendations for minimal cell expansion time frames and prompt patient application to minimise risk of genomic mutations (Wang et al., 2013) (Froelich et al., 2013). Increased need for testing will accompany non-hBMSC cells procured as ATMP from other tissue sources (Sacchetti et al., 2016) and innovative approaches to enhance cell expansion or function, e.g. hypoxic culture conditions can influence chromosome stability (Ueyama et al., 2012) (Bigot et al., 2015) (Anderson et al., 2016). Bioprocessing strategies for large-scale production of hBMSC (Panchalingam et al., 2015) will need to meet regulatory authority product characterization requirements (Mendicino et al., 2014). Suitable biomarker panels for improved prompt assessment of tumorigenic risk pre- and post-engraftment (Goldring et al., 2011) would be of enormous benefit.

Potential problems in obtaining sufficient mitotic spreads from relatively slow-growing primary hBMSC have been largely overcome (Hwang et al., 2013). In most cases, chromosomal G-banding or SKY analysis generally suggested that the karyotype is relatively stable (Chen et al., 2014) and cultured stromal cells from diverse tissue sources aren't prone to neoplastic transformation (Roseti et al., 2014) (Ruan et al., 2014). Nonetheless, a turbulent initial cell culture acclimatization phase may introduce transient genetic errors and karyotypic abnormalities that diminish upon further passage because they fail to confer an evolutionary growth advantage, i.e. detrimental non-sustainable phenotypes inducing cell senescence, growth arrest or apoptosis (Stultz et al., 2016). In such contexts, monitoring the genetic stability of clinical grade hBMSC during primary expansion by SKY karyotyping may more readily help decide upon suitability for use, even if hBMSC-TERT20 tumorigenicity arose in SKY "normal" diploid cells.

Array CGH is a sensitive approach for detecting cytogenetic abnormalities, in particular, the Agilent 400 K human array provided genome-wide CNV profiling without need for amplification or complexity reduction with comprehensive probe coverage enhanced by emphasis on known genes, promoters, miRNAs, pseudoautosomal and telomeric regions. However, since population variation may lead to CNV in roughly 12% of the human genomic DNA of "healthy" cells, setting safety thresholds is not necessarily straightforward. Since aCGH is a method that relies on unique sequence probe hybridisation it has limitations for the detection of repeat sequences, pseudogenes and insight into the orientation or location of insertions, e.g. failing to detect reciprocal translocations. Nonetheless, sensitive detection for intragenic deletions can be obtained among the various arrays available (Askree et al., 2013; Haraksingh et al., 2017).

Defining covert events indicative of tumorigenic predisposition is particularly challenging, given the complexity of cell processes and difficulty in determining the timing of events and their consequences. Despite improved detection from array CGH, interpretation of the significance of the CNV event may be problematical and clinical relevance requires careful interpretation (Hollenbeck et al., 2016) (Savola et al., 2007) (Zhao and Zhao, 2016). To this end the hBMSC-TERT20 model presented several strong points. Independently acquired prior data provided a contextual framework with which to assess CNV. The long-term evolution of the tumorigenic phenotype and contrasting non-tumorigenic closely-matched strains enabled comparisons to identify elusive "pre-neoplastic" events. Verification of CNV persistence in single-cell derived clones provided a test of clonal penetrance and underscored likelihood that the CNV contributed to a persistent proliferative growth advantage.

Our three-year hBMSC-TERT cell expansion model monitored cytogenetic abnormalities and stochastic events leading to tumorigenesis in an isogenic context, providing insights for monitoring ATMP cell cultures for tumorigenic risk. Initial suspicion that loss of the *Ink4a/ARF* locus (*CDKN2A*) was a microdeletion, detectable using PCR amplification yet not by FISH (Serakinci et al., 2004) or SKY (Burns et al., 2008), was confirmed. In addition, aCGH indicated the ~151 kbp microdeletion included an exon of MTAP in addition to CDKN2a and CDKN2b. Such covert 9p21 deletions were responsible for FISH mis-diagnosis in Ewing sarcomas (Savola et al., 2007). Down regulation of MTAP expression concordant with copy number loss has been highlighted in human tumor samples (Kryukov et al., 2016) and osteosarcomas (Jour et al., 2016), generating a PRMT5 metabolic pathway vulnerability. Higher incidence of p16INK4a deletions in cultured cell lines versus primary gliomas, was attributed to a strong cell culture imposed selective pressure (Hartmann et al., 1999). Indeed, p16INK4a expression has close association with contact inhibition of growth in human embryo lung fibroblasts (Wieser et al., 1999) and hBMSC senescence (Shibata et al., 2007). Nevertheless, beyond the culture environment, p16INK4a markedly inhibited the proliferation of aged pancreatic islet stem cells *in vivo* (Krishnamurthy et al., 2006). The specific 9p21 CNV loss in hBMSC-TERT4 was reproduced with a stronger signal in hBMSC-TERT20 cells, suggesting elaboration of a pre-existing genetic aberration. This makes it likely that the 9p21 CNV initiated before the hBMSC-TERT cells were distributed as 1:4 and 1:20 split-ratio-specific populations, making this an earlier event than previously described. Of note, the PCR based method used to detect the 9p21 loss had limited sensitivity and mosaicism within a heterogeneous population could allow variant cells to remain undetected (Baker et al., 2016). Translating a cell specific growth advantage to a detectable change in growth rate of the whole population can be delayed in hBMSC cultures (Garcia et al., 2010) quelling expectation that one may simply detect genetic instability from changes in growth rate kinetics.

Many of the CNV found in all hBMSC-TERT cultures (14/22), might simply reflect a difference pertaining to the comparative reference control DNA, however bioinformatic STRING based interactions indicated that 10 of these ubiquitous CNV contained genes interacting with our hBMSC-TERT20 contextual framework for pathways in cancer. Further interventional experiments beyond the scope of this manuscript would be needed to verify their functional contribution. Focusing, rather, on CNV distributed more heterogeneously among the cell populations, hBMSC-TERT4 cells had one specific 21q11.2 CNV loss, whilst non-tumorigenic hBMSC-TERT20 a 1q44 CNV gain and a 11q13.1 CNV loss that persisted in all the tumorigenic hBMSC- TERT20 subclones. Such a cell strain distribution made the latter two events potential pre-neoplasia biomarkers and notably the 1q44 CNV region harbored the *SMYD3* (Set and MYND domain containing protein 3) oncogene (Mazur et al., 2014) whilst the 11q13.1 CNV region harbored the *MUS81* (Mus81-Eme1 endonuclease) tumor suppressor gene (McPherson et al., 2004). Consistent with a role in the replication stress response (Minocherhomji et al., 2015) and ultrasensitivity to its expression change (Yu et al., 2008), down-regulation of crossover junction endonuclease *MUS81* was a prognostic biomarker for colorectal carcinoma (Wu et al., 2011).

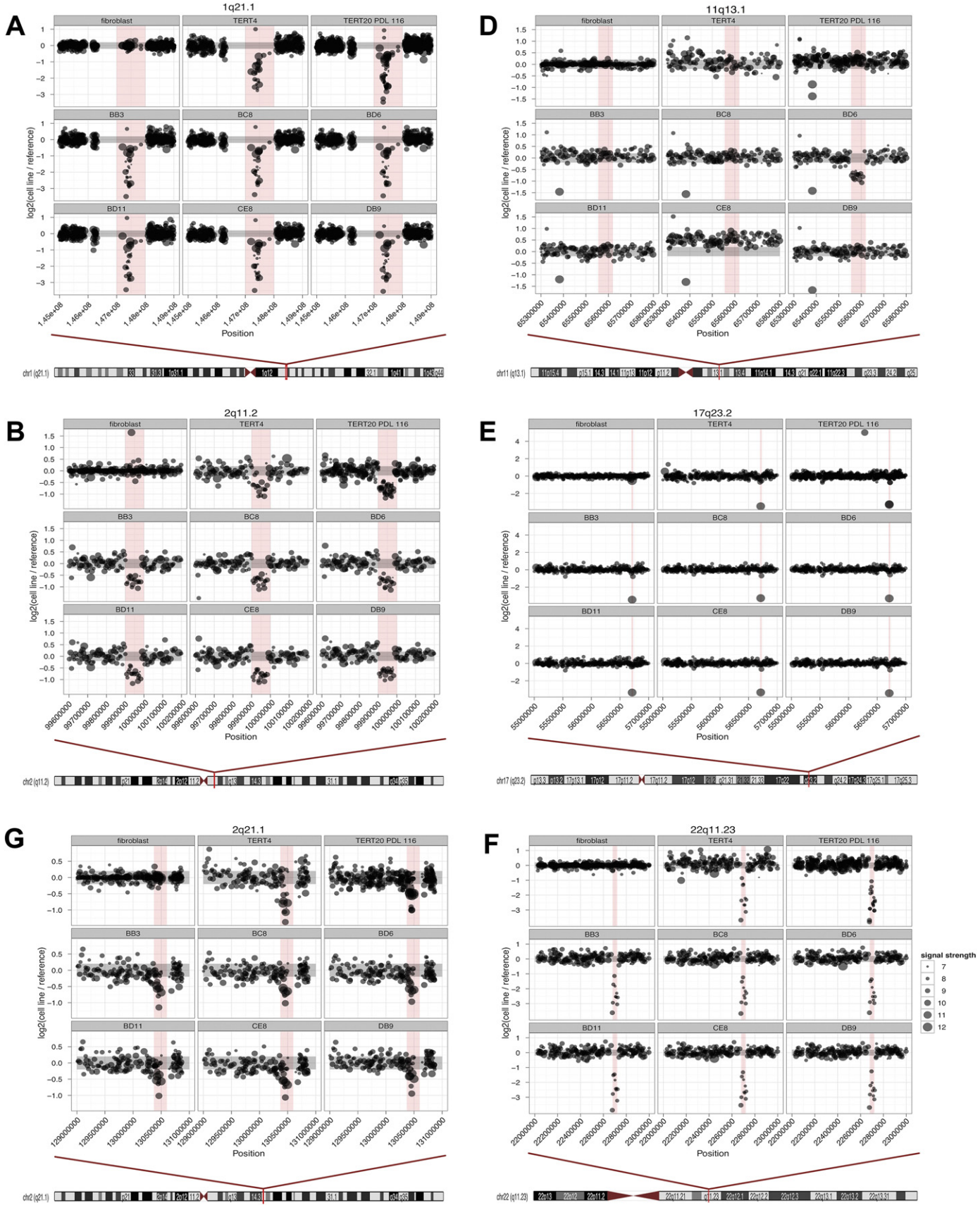
A
1q21.1
fibroblast
TERT4
TERT20 PDL 116
BB3
BC8
BD6
BD11
CE8
DB9
log2(cell line / reference)
Position
chr1 (q21.1)
D
11q13.1
chr11 (q13.1)
B
2q11.2
chr2 (q11.2)
E
17q23.2
chr17 (q23.2)
G
2q21.1
chr2 (q21.1)
F
22q11.23
chr22 (q11.23)
signal strength
7
8
9
10
11
12

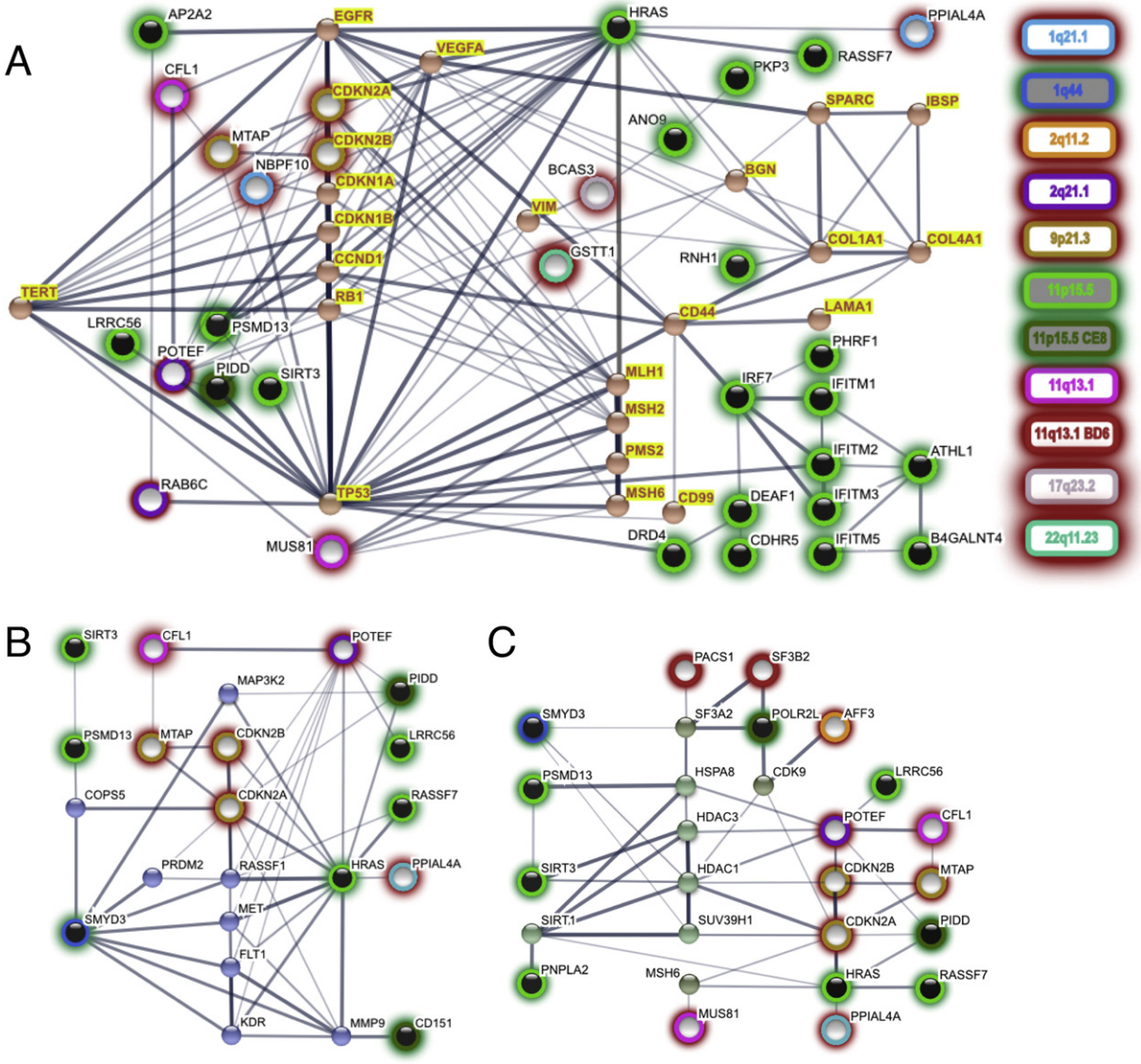

Fig. 6. CNV target gene predicted interactions in contextual frameworks using STRING bioinformatics. A, Graph of interactions within a network derived from prior experimental data for cancer pathways in hBMSC-TERT cells. Highlighted name nodes correspond to proteins and genes characterized by prior experimental data. B, Graph of interactions within a contextual framework derived from CNV 1q44 target SMYD3 predicted interacting proteins (blue nodes). C, Graph of interactions within a contextual framework of epigenetic regulator SIRT1 predicted network interacting proteins (green nodes). Highlighted halo nodes correspond to STRING identified genes within CNV representing a gain (dark node) or loss (pale node) at the colour-coded locus. Interconnecting edges correspond to STRING predicted protein interactions.

CNV events don't necessarily change gene expression (Kuijjer et al., 2012), thus it was reassuring to verify concordant *SMYD3* and *MUS81* expression changes by gene expression analysis to confirm their potential significance. SMYD3 in particular has been shown to be a transcriptional potentiater of multiple cancer promoting genes in liver and colon cancer development (Sarris et al., 2016) with potential to promote the cell cycle (Tsai et al., 2016). Outcomes of increased *SMYD3* expression in cultured cells include reduced contact inhibition and accelerated growth (Luo et al., 2009) (Ren et al., 2011). KEGG analysis of our contextual framework network indicated components of the PI3K/AKT/mTOR signaling network and SMYD3 has been shown to be critical for activation of AKT1 (Yoshioka et al., 2016). Moreover, upregulation of *SMYD3* in bladder cancer can promote cancer progression and activate autophagy (Shen et al., 2016), rendering cancer cells resistant to starvation (Galluzzi et al., 2015), a phenotype highlighted in hBMSC-TERT20 subclones (Burns et al., 2011). Though prevalent in cancers, a role for SMYD3 in sarcomas has yet to be reported, however *p53*-mutant mice only haploinsufficient for *MUS81* were already predisposed to develop sarcomas (Pamidi et al., 2007).

The 11p15.5 CNV gain, closely correlated with hBMSC-TERT strain tumorigenicity, contributed the largest number of potential interactors in our context-defined cancer pathways network. Curiously, despite more extensive full chromosome 11 imbalance, hBMSC-TERT20-CE8 tumors arose latently compared to those for the other clones (Burns et al.,

Fig. 5. CNV interacting with hBMSC-TERT20 contextual framework STRING networks. A, Array CGH profile for 1q21.1 and chromosome 1 ideogram, red bar highlights the ~1000 kbp CNV spanning chr1:147,000,000–148,000,000. B, Array CGH profile for 2q11.2 and chromosome 2 ideogram, red bar highlights the ~100 kbp CNV spanning chr1:99,900,000–100,000,000. C Array CGH profile for 2q21.1 and chromosome 2 ideogram, red bar highlights the ~225 kbp CNV spanning chr2:130,375,000–130,600,000. D, Array CGH profile for 11q13.1 CNV specific to –BD6 cells and chromosome 11 ideogram, red bar highlights the ~65 kbp CNV spanning chr11:65,555,000–65,620,000. E, Array CGH profile for 17q23.2 and chromosome 17 ideogram, red bar highlights the ~50 kbp CNV spanning chr17: 56,700,000–56,750,000. F, Array CGH profile for 22q11.23 and chromosome 22 ideogram, red bar highlights the ~30 kbp CNV spanning chr22:22,685,000–22,715,000. Opposing red arrowheads represent the centrosomic region.

2008). Conspicuous among the many genes affected by the 570 kbp 11p15.5 CNV gain, *HRAS* (Hras proto-oncogene, GTPase) was activated in gliomas by copy number gains more frequently than by activating mutations (Jeuken et al., 2007). Ras activity has context-dependent outcomes, critically dependent on the pre-existing telomerase and *CDKN2A* encoded p16INK4a status of the cells. Though *HRAS* overexpression can induce premature senescence in primary human cells, in clonogenic keratinocytes from the stem cell compartment it could evoke tumorigenic progression (Maurelli et al., 2016). It may seem counterintuitive that hBMSC-TERT4 cells bearing a *KRAS* Q61H activation didn't form tumors, however, the outcome of *KRAS* oncogene expression is highly dependent on cellular context (Guerra et al., 2003) and *KRAS* mutations prove selective only if they occur in cells with an appropriately abrogated defense mechanism (Lee and Bae, 2016). Moreover, the status of the wild-type *HRAS* isoform continues to influence mutant *KRAS* driven signaling (Bentley et al., 2013) and tumorigenic susceptibility may require *KRAS* copy number gains in addition to mutation (Kerr et al., 2016). The hBMSC-TERT4 phenotype was consistent with recent observations that over-activation of *Kras* in immature murine osteoprogenitor cells increased the number of descendent osteoblasts (Papaioannou et al., 2016).

How relevant is the hBMSC-TERT model for guiding ATMP safety? The “extracurricular” additional activities of ectopic hTERT (Cong and Shay, 2008) may not only prevent aneuploidy but also introduce an artefactual bias subverting corrective responses. Extrapolating our results to primary cultures, needs consideration that hBMSC-TERT cells may have an enhanced innate tumorigenic risk. Wayward primary hBMSC may be more readily be detected through karyotypic abnormalities and show growth arrest, senescence or apoptosis as appropriate checkpoint responses that limit tumorigenic risk. Moreover, the time taken for neoplastic evolution in hBMSC-TERT20 cells was well beyond typically contemplated ATMP culture periods (Lechanteur et al., 2016). The hBMSC-TERT20 neoplastic model nonetheless proved that discretely accrued genetic change in cultured cells could not only accelerate growth rate, but also drive neoplasia. With authentic tumorigenesis, the hBMSC- TERT20 model has greatest value in revealing relatively covert yet significant abnormalities that might ordinarily pass undetected in short-term cultures. A rare example of spontaneous tumorigenesis from primary cultured hBMSC verified by STR profiling supports concern for monitoring (Pan et al., 2014), yet even with a “three strikes you're out” model (Vogelstein and Kinzler, 2015), tumorigenesis need not be an inevitable outcome. Even with at least three neoplastic contributors, hTERT expression, the 9p21 microdeletion spanning three checkpoint genes and Kras Q61H activation, subsequently grown hBMSC-TERT4 cells still formed good quality bone tissue upon experimental implantation. Revisiting our well-characterized neoplastic model with aCGH highlighted extra discriminating events in the tumorigenic hBMSC-TERT20 cells, exposed limitations of variously proposed monitoring methods and provided further insights into culture-derived neoplasia. Bioinformatic analysis of CNV locus genes provided strong supportive evidence that chromosomal changes in the diploid cells contributed to pathways engaging co-existent genetic aberrations to establish tumorigenic progression. The model provides a richly annotated experimental framework for future interventional studies verifying the critical pathways driving neoplasia arisen in stem cells.

The hBMSC-TERT model can guide rational design for improved predictive genomics (Wang et al., 2015) by introducing novel biomarkers of neoplastic risk for tailored cost-effective arrays with enhanced probe coverage dedicated to safe stem cell expansion (Pan et al., 2014) and complementary platforms for epigenetic monitoring (Wagner et al., 2016). Our direct experimental evidence that mutation of stem cells with convergence of extrinsic factors can together create conditions to drive tumorigenesis agrees with what has been learned from mapping cancer risk *in vivo* (Zhu et al., 2016; Sheffield et al., 2017).

Supplementary data to this article can be found online at https://doi.org/10.1016/j.scr.2017.09.006.

Acknowledgements

We thank Anne Grethe Sørensen, Lone Christiansen and Pia Friis for technical assistance, Jacob Bentzon, Per Guldberg and Henrik D. Schrøder for helpful discussion. This work was supported by the Lunbeck foundation, Karen Elise Jensen's Fond, Novo Nordisk Foundation (NNF15OC0016284), Gross M. Brogaard og Hustru Foundation, Jacob Madsen og Hustru Foundation, an infrastructure grant from the Technical University of Denmark and Danish Lægeforening Research Foundation.

Disclosure of potential conflicts of interest

The authors declare no potential conflict of interest.

References

Abdallah, B.M., Haack-Sorensen, M., Burns, J.S., Elsnab, B., Jakob, F., Hokland, P., et al., 2005. Maintenance of differentiation potential of human bone marrow mesenchymal stem cells immortalized by human telomerase reverse transcriptase gene despite [corrected] extensive proliferation. Biochem. Biophys. Res. Commun. 326, 527–538.

Abercrombie, M., 1970. Contact inhibition in tissue culture. In Vitro 6, 128–142.

Anderson, D.E., Markway, B.D., Bond, D., McCarthy, H.E., Johnstone, B., 2016. Responses to altered oxygen tension are distinct between human stem cells of high and low chondrogenic capacity. Stem Cell Res Ther 7, 154.

Askree, S.H., Chin, E.L., Bean, L.H., Coffee, B., Tanner, A., Hegde, M., 2013. Detection limit of intragenic deletions with targeted array comparative genomic hybridization. BMC Genet. 14, 116.

Baker, D., Hirst, A.J., Gokhale, P.J., Juarez, M.A., Williams, S., Wheeler, M., et al., 2016. Detecting genetic mosaicism in cultures of human pluripotent stem cells. Stem Cell Rep. 7, 998–1012.

Bentley, C., Jurinka, S.S., Kljavin, N.M., Vartanian, S., Ramani, S.R., Gonzalez, L.C., et al., 2013. A requirement for wild-type Ras isoforms in mutant KRas-driven signalling and transformation. Biochem. J. 452, 313–320.

Bigot, N., Mouche, A., Preti, M., Loisel, S., Renoud, M.L., Le Guével, R., et al., 2015. Hypoxia differentially modulates the genomic stability of clinical-grade ADSCs and BM-MSCs in long-term culture. Stem Cells 33, 3608–3620.

Black, J.B., Adler, A.F., Wang, H.G., D'Ippolito, A.M., Hutchinson, H.A., Reddy, T.E., et al., 2016. Targeted epigenetic remodeling of endogenous loci by CRISPR/Cas9-based transcriptional activators directly converts fibroblasts to neuronal cells. Cell Stem Cell 19, 406–414.

Burns, J.S., Abdallah, B.M., Guldberg, P., Rygaard, J., Schroder, H.D., Kassem, M., 2005. Tumorigenic heterogeneity in cancer stem cells evolved from long-term cultures of telomerase-immortalized human mesenchymal stem cells. Cancer Res. 65, 3126–3135.

Burns, J.S., Abdallah, B.M., Schroder, H.D., Kassem, M., 2008. The histopathology of a human mesenchymal stem cell experimental tumor model: support for an hMSC origin for Ewing's sarcoma? Histol. Histopathol. 23, 1229–1240.

Burns, J.S., Rasmussen, P.L., Larsen, K.H., Schroder, H.D., Kassem, M., 2010. Parameters in three-dimensional osteospheroids of telomerized human mesenchymal (stromal) stem cells grown on osteoconductive scaffolds that predict *in vivo* bone-forming potential. Tissue Eng. Part A 16, 2331–2342.

Burns, J.S., Kristiansen, M., Kristensen, L.P., Larsen, K.H., Nielsen, M.O., Christiansen, H., et al., 2011. Decellularized matrix from tumorigenic human mesenchymal stem cells promotes neovascularization with galectin-1 dependent endothelial interaction. PLoS One 6, e21888.

Caplan, A.I., 2017. Mesenchymal stem cells: time to change the name. Stem Cells Transl. Med. 6, 1445–1451.

Chen, G., Yue, A., Ruan, Z., Yin, Y., Wang, R., Ren, Y., et al., 2014. Monitoring the biology stability of human umbilical cord-derived mesenchymal stem cells during long-term culture in serum-free medium. Cell Tissue Bank. 15, 513–521.

Cong, Y., Shay, J.W., 2008. Actions of human telomerase beyond telomeres. Cell Res. 18, 725–732.

Elliott, A.M., Elliott, K.A., Kammesheidt, A., 2010. High resolution array-CGH characterization of human stem cells using a stem cell focused microarray. Mol. Biotechnol. 46, 234–242.

Ferreira, R.J., Irioda, A.C., Cunha, R.C., Francisco, J.C., Guarita-Souza, L.C., Srikanth, G.V., et al., 2012. Controversies about the chromosomal stability of cultivated mesenchymal stem cells: their clinical use is it safe? Curr. Stem Cell Res. Ther. 7, 356–363.

Froelich, K., Mickler, J., Steusloff, G., Technau, A., Ramos Tirado, M., Scherzed, A., et al., 2013. Chromosomal aberrations and deoxyribonucleic acid single-strand breaks in adipose-derived stem cells during long-term expansion in vitro. Cytotherapy 15, 767–781.

Furlani, D., Li, W., Pittermann, E., Klopsch, C., Wang, L., Knopp, A., et al., 2009. A transformed cell population derived from cultured mesenchymal stem cells has no functional effect after transplantation into the injured heart. Cell Transplant. 18, 319–331.

Galluzzi, L., Pietrocola, F., Bravo-San Pedro, J.M., Amaravadi, R.K., Baehrecke, E.H., Cecconi, F., et al., 2015. Autophagy in malignant transformation and cancer progression. EMBO J. 34, 856–880.

Garcia, S., Bernad, A., Martín, M.C., Cigudosa, J.C., Garcia-Castro, J., de la Fuente, R., 2010. Pitfalls in spontaneous in vitro transformation of human mesenchymal stem cells. Exp. Cell Res. 316, 1648–1650.

Goldring, C.E., Duffy, P.A., Benvenisty, N., Andrews, P.W., Ben-David, U., Eakins, R., et al., 2011. Assessing the safety of stem cell therapeutics. Cell Stem Cell 8, 618–628.
Guerra, C., Mijimolle, N., Dhawahir, A., Dubus, P., Barradas, M., Serrano, M., et al., 2003. Tumor induction by an endogenous K-ras oncogene is highly dependent on cellular context. Cancer Cell 4, 111–120.
György, B., Hung, M.E., Breakefield, X.O., Leonard, J.N., 2015. Therapeutic applications of extracellular vesicles: clinical promise and open questions. Annu. Rev. Pharmacol. Toxicol. 55, 439–464.
Hamamoto, R., Furukawa, Y., Morita, M., Iimura, Y., Silva, F.P., Li, M., et al., 2004. SMYD3 encodes a histone methyltransferase involved in the proliferation of cancer cells. Nat. Cell Biol. 6, 731–740.
Haraksingh, R.R., Abyzov, A., Urban, A.E., 2017. Comprehensive performance comparison of high-resolution array platforms for genome-wide Copy Number Variation (CNV) analysis in humans. BMC Genomics 18, 321.
Hartmann, C., Kluwe, L., Lücke, M., Westphal, M., 1999. The rate of homozygous CDKN2A/p16 deletions in glioma cell lines and in primary tumors. Int. J. Oncol. 15, 975–982.
Hollenbeck, D., Williams, C.L., Drazba, K., Descartes, M., Korf, B.R., Rutledge, S.L., et al., 2016. Clinical relevance of small copy-number variants in chromosomal microarray clinical testing. Genet. Med. 19, 377–385.
Hwang, S.M., See, C.J., Choi, J., Kim, S.Y., Choi, Q., Kim, J.A., et al., 2013. The application of an in situ karyotyping technique for mesenchymal stromal cells: a validation and comparison study with classical G-banding. Exp. Mol. Med. 45, e68.
Jeuken, J., van den Broecke, C., Gijsen, S., Boots-Sprenger, S., Wesseling, P., 2007. RAS/RAF pathway activation in gliomas: the result of copy number gains rather than activating mutations. Acta Neuropathol. 114, 121–133.
Jour, G., Wang, L., Middha, S., Zehir, A., Chen, W., Sadowska, J., et al., 2016. The molecular landscape of extraskeletal osteosarcoma: a clinicopathological and molecular biomarker study. J. Pathol. Clin. Res. 2, 9–20.
Kanehisa, M., Sato, Y., Kawashima, M., Furumichi, M., Tanabe, M., 2016. KEGG as a reference resource for gene and protein annotation. Nucleic Acids Res. 44, D457–62.
Kerr, E.M., Gaude, E., Turrell, F.K., Frezza, C., Martins, C.P., 2016. Mutant Kras copy number defines metabolic reprogramming and therapeutic susceptibilities. Nature 531, 110–113.
Krishnamurthy, J., Ramsey, M.R., Ligon, K.L., Torrice, C., Koh, A., Bonner-Weir, S., et al., 2006. p16INK4a induces an age-dependent decline in islet regenerative potential. Nature 443, 453–457.
Kryukov, G.V., Wilson, F.H., Ruth, J.R., Paulk, J., Tsherniak, A., Marlow, S.E., et al., 2016. MTAP deletion confers enhanced dependency on the PRMT5 arginine methyltransferase in cancer cells. Science 351, 1214–1218.
Kuijjer, M.L., Rydbeck, H., Kresse, S.H., Buddingh, E.P., Lid, A.B., Roelofs, H., et al., 2012. Identification of osteosarcoma driver genes by integrative analysis of copy number and gene expression data. Genes Chromosom. Cancer 51, 696–706.
Lechanteur, C., Briquet, A., Giet, O., Delloye, O., Baudoux, E., Beguin, Y., 2016. Clinical-scale expansion of mesenchymal stromal cells: a large banking experience. J. Transl. Med. 14, 145.
Lee, Y.S., Bae, S.C., 2016. How do K-RAS-activated cells evade cellular defense mechanisms. Oncogene 35, 827–832.
Liu, C., Fang, X., Ge, Z., Jalink, M., Kyo, S., Björkholm, M., et al., 2007. The telomerase reverse transcriptase (hTERT) gene is a direct target of the histone methyltransferase SMYD3. Cancer Res. 67, 2626–2631.
Luo, X.G., Xi, T., Guo, S., Liu, Z.P., Wang, N., Jiang, Y., et al., 2009. Effects of SMYD3 overexpression on transformation, serum dependence, and apoptosis sensitivity in NIH3T3 cells. IUBMB Life 61, 679–684.
Lupberger, J., Kreuzer, K.A., Baskaynak, G., Peters, U.R., le Coutre, P., Schmidt, C.A., 2002. Quantitative analysis of beta-actin, beta-2-microglobulin and porphobilinogen deaminase mRNA and their comparison as control transcripts for RT-PCR. Mol. Cell. Probes 16, 25–30.
Maurelli, R., Tinaburri, L., Gangi, F., Bondanza, S., Severi, A.L., Scarponi, C., et al., 2016. The role of oncogenic Ras in human skin tumorigenesis depends on the clonogenic potential of the founding keratinocytes. J. Cell Sci. 129, 1003–1017.
Mazur, P.K., Reynoird, N., Khatri, P., Jansen, P.W., Wilkinson, A.W., Liu, S., et al., 2014. SMYD3 links lysine methylation of MAP3K2 to Ras-driven cancer. Nature 510, 283–287.
McPherson, J.P., Lemmers, B., Chahwan, R., Pamidi, A., Migon, E., Matysiak-Zablocki, E., et al., 2004. Involvement of mammalian Mus81 in genome integrity and tumor suppression. Science 304, 1822–1826.
Mendicino, M., Bailey, A.M., Wonnacott, K., Puri, R.K., Bauer, S.R., 2014. MSC-based product characterization for clinical trials: an FDA perspective. Cell Stem Cell 14, 141–145.
Minocherhomji, S., Ying, S., Bjerregaard, V.A., Bursomanno, S., Aleliunaite, A., Wu, W., et al., 2015. Replication stress activates DNA repair synthesis in mitosis. Nature 528, 286–290.
Pamidi, A., Cardoso, R., Hakem, A., Matysiak-Zablocki, E., Poonepalli, A., Tamblyn, L., et al., 2007. Functional interplay of p53 and Mus81 in DNA damage responses and cancer. Cancer Res. 67, 8527–8535.
Pan, Q., Fouraschen, S.M., de Ruiter, P.E., Dinjens, W.N., Kwekkeboom, J., Tilanus, H.W., et al., 2014. Detection of spontaneous tumorigenic transformation during culture expansion of human mesenchymal stromal cells. Exp. Biol. Med. 239, 105–115.
Panchalingam, K.M., Jung, S., Rosenberg, L., Behie, L.A., 2015. Bioprocessing strategies for the large-scale production of human mesenchymal stem cells: a review. Stem Cell Res Ther 6, 225.
Papaioannou, G., Mirzamohammadi, F., Kobayashi, T., 2016. Ras signaling regulates osteoprogenitor cell proliferation and bone formation. Cell Death Dis. 7, e2405.
Quarto, R., Mastrogiacomo, M., Cancedda, R., Kutepov, S.M., Mukhachev, V., Lavroukov, A., et al., 2001. Repair of large bone defects with the use of autologous bone marrow stromal cells. N. Engl. J. Med. 344, 385–386.
Ren, T.N., Wang, J.S., He, Y.M., Xu, C.L., Wang, S.Z., Xi, T., 2011. Effects of SMYD3 over-expression on cell cycle acceleration and cell proliferation in MDA-MB-231 human breast cancer cells. Med. Oncol. 28 (Suppl. 1), S91–8.
Robey, P., 2017. "Mesenchymal stem cells": fact or fiction, and implications in their therapeutic use. F1000Res. 6.
Roseti, L., Serra, M., Canella, F., Munno, C., Tosi, A., Zuntini, M., et al., 2014. In vitro gene and chromosome characterization of expanded bone marrow mesenchymal stem cells for musculo-skeletal applications. Eur. Rev. Med. Pharmacol. Sci. 18, 3702–3711.
Ruan, Z.B., Zhu, L., Yin, Y.G., Chen, G.C., 2014. Karyotype stability of human umbilical cord-derived mesenchymal stem cells during in vitro culture. Exp. Ther. Med. 8, 1508–1512.
Sacchetti, B., Funari, A., Remoli, C., Giannicola, G., Kogler, G., Liedtke, S., et al., 2016. No identical "mesenchymal stem cells" at different times and sites: human committed progenitors of distinct origin and differentiation potential are incorporated as adventitial cells in microvessels. Stem Cell Rep. 6, 897–913.
Saito, S., Morita, K., Kohara, A., Masui, T., Sasao, M., Ohgushi, H., et al., 2011. Use of BAC array CGH for evaluation of chromosomal stability of clinically used human mesenchymal stem cells and of cancer cell lines. Hum. Cell 24, 2–8.
Sarris, M.E., Moulos, P., Haroniti, A., Giakountis, A., Talianidis, I., 2016. Smyd3 is a transcriptional potentiator of multiple cancer-promoting genes and required for liver and colon cancer development. Cancer Cell 29, 354–366.
Savola, S., Nardi, F., Scotlandi, K., Picci, P., Knuutila, S., 2007. Microdeletions in 9p21.3 induce false negative results in CDKN2A FISH analysis of Ewing sarcoma. Cytogenet. Genome Res. 119, 21–26.
Serakinci, N., Guldberg, P., Burns, J.S., Abdallah, B., Schrodder, H., Jensen, T., et al., 2004. Adult human mesenchymal stem cell as a target for neoplastic transformation. Oncogene 23, 5095–5098.
Sheffield, N.C., Pierron, G., Klughammer, J., Datlinger, P., Schönegger, A., Schuster, M., et al., 2017. DNA methylation heterogeneity defines a disease spectrum in Ewing sarcoma. Nat. Med. 23, 386–395.
Shen, B., Tan, M., Mu, X., Qin, Y., Zhang, F., Liu, Y., et al., 2016. Upregulated SMYD3 promotes bladder cancer progression by targeting BCLAF1 and activating autophagy. Tumour Biol. 37, 7371–7381.
Shibata, K.R., Aoyama, T., Shima, Y., Fukiage, K., Otsuka, S., Furu, M., et al., 2007. Expression of the p16INK4A gene is associated closely with senescence of human mesenchymal stem cells and is potentially silenced by DNA methylation during in vitro expansion. Stem Cells 25, 2371–2382.
Simonsen, J.L., Rosada, C., Serakinci, N., Justesen, J., Stenderup, K., Rattan, S.I., et al., 2002. Telomerase expression extends the proliferative life-span and maintains the osteogenic potential of human bone marrow stromal cells. Nat. Biotechnol. 20, 592–596.
Stultz, B.G., McGinnis, K., Thompson, E.E., Lo Surdo, J.L., Bauer, S.R., Hursh, D.A., 2016. Chromosomal stability of mesenchymal stromal cells during in vitro culture. Cytotherapy 18, 336–343.
Szklarczyk, D., Franceschini, A., Wyder, S., Forslund, K., Heller, D., Huerta-Cepas, J., et al., 2015. STRING v10: protein-protein interaction networks, integrated over the tree of life. Nucleic Acids Res. 43, D447–52.
Tsai, C.H., Chen, Y.J., Yu, C.J., Tzeng, S.R., Wu, I.C., Kuo, W.H., et al., 2016. SMYD3-Mediated H2A.Z.1 Methylation Promotes Cell Cycle and Cancer Proliferation. Cancer Res. 76, 6043–6053.
Ueyama, H., Horibe, T., Hinotsu, S., Tanaka, T., Inoue, T., Urushihara, H., et al., 2012. Chromosomal variability of human mesenchymal stem cells cultured under hypoxic conditions. J. Cell. Mol. Med. 16, 72–82.
Vogelstein, B., Kinzler, K.W., 2015. The path to cancer—three strikes and you're out. N. Engl. J. Med. 373, 1895–1898.
Wagner, W., Frobel, J., Goetzke, R., 2016. Epigenetic quality check - how good are your mesenchymal stromal cells. Epigenomics 8, 889–894.
Wang, Y., Zhang, Z., Chi, Y., Zhang, Q., Xu, F., Yang, Z., et al., 2013. Long-term cultured mesenchymal stem cells frequently develop genomic mutations but do not undergo malignant transformation. Cell Death Dis. 4, e950.
Wang, E., Zaman, N., Mcgee, S., Milanese, J.S., Masoudi-Nejad, A., O'Connor-McCourt, M., 2015. Predictive genomics: a cancer hallmark network framework for predicting tumor clinical phenotypes using genome sequencing data. Semin. Cancer Biol. 30, 4–12.
Wieser, R.J., Faust, D., Dietrich, C., Oesch, F., 1999. p16INK4 mediates contact-inhibition of growth. Oncogene 18, 277–281.
Wu, F., Shirahata, A., Sakuraba, K., Kitamura, Y., Goto, T., Saito, M., et al., 2011. Downregulation of Mus81 as a novel prognostic biomarker for patients with colorectal carcinoma. Cancer Sci. 102, 472–477.
Yam, G.H., Yusoff, N.Z., Goh, T.W., Setiawan, M., Lee, X.W., Liu, Y.C., et al., 2016. Decellularization of human stromal refractive lenticules for corneal tissue engineering. Sci Rep 6, 26339.
Yoshioka, Y., Suzuki, T., Matsuo, Y., Nakakido, M., Tsurita, G., Simone, C., et al., 2016. SMYD3-mediated lysine methylation in the PH domain is critical for activation of AKT1. Oncotarget 7, 75023–75037.
Yu, K., Ganesan, K., Tan, L.K., Laban, M., Wu, J., Zhao, X.D., et al., 2008. A precisely regulated gene expression cassette potently modulates metastasis and survival in multiple solid cancers. PLoS Genet. 4, e1000129.
Zhao, M., Zhao, Z., 2016. Concordance of copy number loss and down-regulation of tumor suppressor genes: a pan-cancer study. BMC Genomics 17 (Suppl. 7), 532.
Zhu, L., Finkelstein, D., Gao, C., Shi, L., Wang, Y., López-Terrada, D., et al., 2016. Multi-organ Mapping of Cancer Risk. Cell 166, 1132–1146.e7.